Journal of Applied Mechanics Vol.13, pp.601-609 (August 2010) JSCE

Nonlinear seismic finite element analysis of soil-pile-superstructure interaction

Mahmoud N. Hussien*, Tetsuo Tobita**, and Susumu Iai***

* PhD student Dept. of Civil and Earth Resources Eng. Kyoto University (Katsura Campus, Nishikyo-ku, Kyoto, 615-8540)
** Member Dr. of Eng. Ass. Prof. Disaster Prevention Research Institute, Kyoto University (Gokasho, Uji, Kyoto, 611–0011)
** * Member Dr. of Eng. Prof. Disaster Prevention Research Institute, Kyoto University (Gokasho, Uji, Kyoto, 611–0011)

Nonlinear seismic analyses using the 2-D finite element (FE) method are compared to the results of shaking table centrifuge model tests of pile-supported structures in a dense sand profile. The soil-pile interaction in 3-D is idealized in 2-D type using soil-pile interaction springs with hysteretic nonlinear load displacement relationships. While the conventional spring elements used in the analysis of soil-pile interactions are embedded in the same plane of the 2-D FE analysis domain, the soil-pile interaction spring used in this study is a spring that connects a free pile to a 2-D cross section of soil. The model is shaken using sinusoidal accelerations with different amplitudes and different frequencies. The computed time histories of ground surface acceleration, pile cap acceleration, and superstructure acceleration were consistent with those obtained from experiments. However, some calibration in the numerical modeling may be required to have more consistent results on the bending moments.

Key Words: *Finite element, pile, dynamic bending moment, centrifuge*

1. Introduction

Recently, estimation of the seismic response of piles and piles supporting structures has received considerable attention especially in seismic areas such as Japan. The lack of well-documented and well-instrumented full-scale case history data and post-earthquake investigations of pile failures has motivated researchers to perform centrifuge and shaking table model tests to augment the field case histories with laboratory data obtained under controlled conditions. The results of these tests provide a good basis for calibration and validation of the available analytical methods developed for seismic soil-pile-superstructure interaction (SSPSI) problems. The available procedures of analyzing SSPSI have included those based on simplified interactions models such as the beam on dynamic Winkler Foundation approach [1-3], as well as those based on more rigorous FEM [4-6] or BEM [7, 8] formulations. These methods utilize either simplified two-step methods that uncouple the superstructure and foundation portions [9-11] or a fully coupled SSPSI system in a single step [12-14]. Although the former provides insights as to the distinct role of inertial and kinematic interaction, the latter gives a direct and more convenient estimation of the complete system response. The coupled 3-D FE approach is most representative of the SSPSI system, but is computationally intensive and time consuming.

Under moderate and strong seismic loading, pile foundations undergo large displacements and the behavior of the soil-pile system can be strongly nonlinear. Although soil-pile interaction with small displacement may be relatively easily analyzed using 3-D finite element technique, soil-pile interaction with large displacement may pose a challenge to engineers and researchers. For example, highly nonlinear nature of soil can result in strain concentration at soil-pile surface, posing difficulty in numerical analysis that may have worked well in linear analysis. Ozutsumi et al. [15] proposed a method to idealize the soil-pile interaction in 3-D into the 2-D type using soil-pile interaction springs with hysteretic nonlinear load displacement relationships. Although the validity of this method was confirmed by Tamari et al. [16], the current paper extends the analysis to include the superstructure in order to evaluate the effects of SPSI for a fully coupled system.

This article presents comparisons of nonlinear seismic FE analyses using the interaction spring proposed by Ozutsumi et al. [15] and shaking table centrifuge model tests of a single pile supporting simple structure founded on a homogeneous dense sand layer over rigid rock. A schematic view of the system under investigation is shown in Fig. 1. Details of centrifuge models and the FE models are briefly summarized. Then the

results of the FE and centrifuge models are compared in terms of time histories of soil and structural responses. The test results of centrifuge are presented in terms of prototype unless otherwise stated. The results show that the FE models were able to reasonably capture the essential features of soil (ground surface acceleration) and structural response (pile cap displacement, pile cap acceleration, superstructure acceleration, and the increase of bending moment profile) for the range of conditions covered in the experiments.

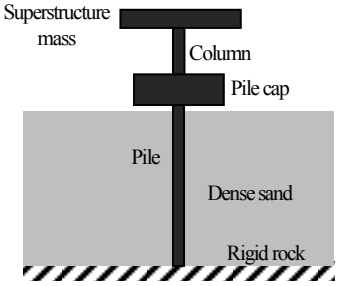

Fig.1 A schematic view of the system under investigation

2. Centrifuge Tests

The model tests were performed using the geotechnical centrifuge at the Disaster Prevention Research Institute, Kyoto University (DPRI-KU). The centrifuge has a radius of 2.5 m and consists of a balanced arm with dual swing platforms. The maximum capacity is 24 g-tons with a maximum centrifugal acceleration of 200 g. A shake table driven unidirectionally by a servo hydraulic actuator is attached to a platform and it is controlled through a personal computer (PC) on the centrifuge arm. All the equipment necessary for shake table control is put together on the arm. The PC is accessible during flight from a PC in the control room through wireless LAN and "Remote Desktop Environment". The shake table has the capacity of 15 kN, 10g and ± 2.5 mm in maximum force, acceleration and displacement, respectively (Tobita et al., 2006) [17]. All tests were carried out in the centrifugal acceleration field of 40g using a rigid soil container with inner dimension of 0.45 m (L) × 0.15 m (W) × 0.29 m (H).

The model ground in this study was made of Silica sand No. 7 having the physical and mechanical properties shown in Table 1 and the particle size distribution curve shown in Fig. 2. A dry sand deposit was prepared by air pluvation. After fixing the pile in a bottom plate in the soil container base, silica sand was rained in 1 g field using a hopper fixed at the specified height until the sand deposit formed 11.6 m thick deposit (290 mm in model scale). The sand deposit was then consolidated in 40 g centrifugal acceleration field for 5 min. By measuring the heights of the ground surface after the consolidation, relative density was obtained as 85%. The soil was instrumented with accelerometers at different depths.

The pile was placed in the model before the soil was pluviated, attempting to simulate a pile installed with minimal disturbance to the surrounding soil, as may be the case when a pile inserted into a pre-augered hole. Seven strain gauges were placed at different locations along the pile to measure bending moments. The single pile was supporting a simple structure consisted of pile cap, column, and superstructure mass as shown in Fig. 1. The pile cap and the superstructure mass were instrumented with LDTs and accelerometers to measure their displacements and accelerations. Material properties of model pile, pile cap, column, and superstructure mass used in this study are shown in Table 2, Table 3, Table 4, and Table 5 respectively. For the pile cap and the superstructure mass, the centrifuge scaling relations were applied based on mass and stiffness.

Table 1 Physical properties of Silica sand No. 7

e_{max}	e_{min}	D_{50}(mm)	Uc	Gs
1.19	0.710	0.13	1.875	2.66

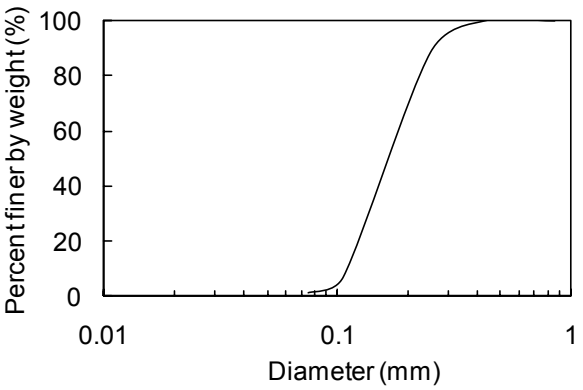

Fig. 2 Particle size distribution curve for Silica sand No.7

Table 2 Properties of pile modeling

	Steel tube		
	Model scale	Prototype scale	Units
Length	0.29	11.6	m
Outer diameter	10	400	mm
Wall thickness	0.75	30	mm
Young's modulus	206	206	GPa
2nd moment of inertia	2.35×10^{2}	6.00×10^{8}	mm^4
Bending stiffness	48.41	1.24×10^{8}	MN-mm^2

Table 3 Properties of pile cap modeling

	Model	Prototype	Units
Mass	0.3792	24231	kg
2nd moment of inertia	9.0×10^{4}	2.33×10^{11}	mm^4
Bending stiffness	1.85×10^{4}	4.75×10^{10}	MN-mm^2

Three sinusoidal waves as input base accelerations with different amplitudes and different frequencies as shown in Table

6 were applied in series (Each shaking event was stronger than the previous one) to the system without the superstructure mass. Then the superstructure mass was added and the three input base accelerations were applied to the system with the same previous manner.

Table 4 Properties of column modeling

	Steel tube		
	Model scale	Prototype scale	Units
Length	0.075	3.0	m
Outer diameter	10	400	mm
Wall thickness	0.75	30	mm
Young's modulus	206	206	GPa
2nd moment of inertia	2.35×10^{2}	6.00×10^{8}	mm^4
Bending stiffness	48.41	1.24×10^{8}	$MN\text{-}mm^2$

Table 5 Properties of superstructure mass modeling

	Model	Prototype	Units
Mass	0.297	19008	kg
2nd moment of inertia	1.41×10^{4}	3.61×10^{10}	mm^4
Bending stiffness	2.90×10^{3}	7.42×10^{9}	$MN\text{-}mm^2$

Table 6 Input base motions

Base acceleration	Max amplitude (g)	Frequency (Hz)
1	0.005	0.1
2	0.084	0.5
3	0.317	1.0

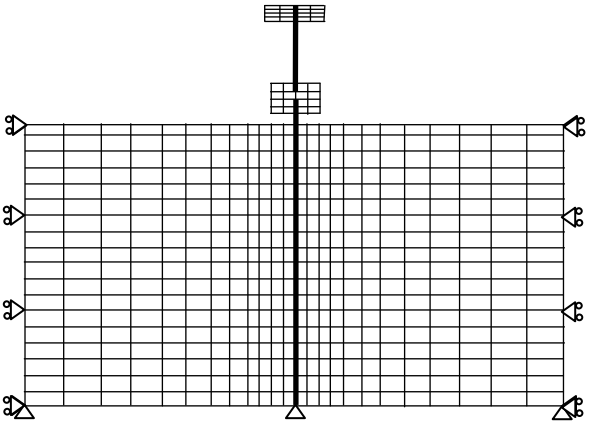

Fig. 3 General layout and meshing of the FE model.

3. Finite Element Model

3.1 Finite elements

The 2-D FE program **FLIP** (**F**inite element analysis program for **LI**quefaction **P**rocess) (Iai et al. 1992)[18] was employed in this study. Figure 3 shows the general layout and meshing of the FE model. Side boundary displacements were fixed in the horizontal direction, while those at the bottom boundary were fixed in both the horizontal and vertical directions to simulate the condition of the centrifuge tests.

3.2 Soil model

The soil continum was modeled using 2D quad elements with a hyperbolic-type multiple shear mechanism (Iai et al. 1992). The basic form of the constitutive relation is given by

$$\{d\sigma'\} = [D]\left(\{d\varepsilon\} - \{d\varepsilon_p\}\right) \tag{1}$$

where σ' is effective stress. ε and ε_p are the strain and the plastic volumetric strain generated by the transient and cyclic loads, respectively. The stiffness matrix is given by

$$[D] = K\{n^{(0)}\}\{n^{(0)}\}^T + \sum_{i=1}^{I} G_{L/U}^{(i)}\{n^{(i)}\}\{n^{(i)}\}^T \tag{2}$$

where the first term represents the volumetric mechanism with an elastic tangent bulk modulus of soil skeleton K and the direction vector is expressed as

$$\{n^{(0)}\}^T = \{1 \quad 1 \quad 0\} \tag{3}$$

and the second term represents the multiple shear mechanism without a volume change. Each mechanism i=1,....,I represents a virtual simple shear mechanism where each simple shear plane is oriented at an angle $\theta i/2+\pi/4$ relative to the x axis. The tangential shear modulus $G_{L/U}^{(i)}$ represents the hyperbolic stress strain relationship with hysteresis characteristics. The direction vectors for the multiple shear mechanism are given by

$$\{n^{(i)}\}^T = \{\cos\theta_i \quad -\cos\theta_i \quad \sin\theta_i\} \text{ (for } i=1,....,I) \tag{4}$$

$$\theta_i = (i-1)\Delta\theta \quad \text{(for } i=1,....,I) \tag{5}$$

$$\Delta\theta = \pi / I \quad \text{(for } i=1,....,I) \tag{6}$$

The loading L and unloading U for the shear mechanism are separately defined for each mechanism by the sign of $\{n^{(i)}\}^T\{d\varepsilon\}$. Each tangent modulus $G_{L/U}^{(i)}$ depends on the present state and the history of each virtual simple shear strain $\gamma^{(i)}$. The virtual shear stress $q^{(i)}$ is introduced as the shear resistance variable, which is defined per unit angle θ for mechanism i. If the inherent soil fabric is assumed to be isotropic, then the virtual simple shear mechanism is defined by a hyperbolic relation under a constant confining stress as

$$q^{(i)} = \frac{\gamma^{(i)} / \gamma_v}{1 + \left|\gamma^{(i)} / \gamma_v\right|} q_v \tag{7}$$

where q_v and γ_v are the parameters that define the hyperbolic relationship and are called the virtual shear strength and virtual reference strain, respectively. The virtual tangent shear moduli are obtained for the initial loading as

$$G_{L/U}^{(i)} = \frac{\gamma^{(i)} / \gamma_v}{\left(1 + \left|\gamma^{(i)} / \gamma_v\right|\right)^2} \frac{q_v}{\gamma_v} \Delta\theta \tag{8}$$

The relationships between parameters q_v and γ_v and the macroscopic shear strength τ_m, and shear modulus G_m can be written as

$$G_m = \frac{q_v}{\gamma_v} \sum_{i=1}^{I} \sin^2 \theta_i \, \Delta\theta \tag{9}$$

$$\tau_m = q_v \sum_{i=1}^{I} \sin^2 \theta_i \, \Delta\theta \tag{10}$$

The shear modulus G_m, which corresponds to the effective mean stress σ'_m is related to the initial shear modulus G_{ma}, which corresponds to the initial effective mean stress σ'_{ma}, as

$$G_m = G_{ma} \left(\frac{\sigma'_m}{\sigma'_{ma}}\right)^{0.5} \tag{11}$$

The shear strength is related to the angle of internal friction φ_f and cohesion c as

$$\tau_m = c \cos\varphi_f - \sigma'_m \sin\varphi_f \tag{12}$$

Parameters for sand used in the FE analysis were determined referring to the results of laboratory tests on Silica sand No. 7 as shown in Table 7. The bulk modulus of the soil skeleton *K* was determined assuming a Poisson's ratio υ of 0.33.

3.3 Pile and column model

Bilinear one-dimensional beam elements with three degrees of freedom per node were used to model the pile and the column. Normal force, shear force, and bending moment for each element were obtained directely from the finite element program. Table 8 defines the model parameters of pile and column elements. Parameters for the pile and the column were from the industrial standard .

3.4 Pile cap and superstructure mass model

Table 7 Model parameters for soil elements.

Density, ρ (t/m^3)	G_{ma} (kPa)	υ	σ'_{ma} (kPa)	φ_f (deg)	H_{max}
1.5	5.1×10^4	0.33	57.11	38	0.20

Table 8 Model parameters for pile and column elements.

Gs (kPa)	υ	ρ (t/m^3)	Initial flexural rigidity (kPa)	Flexural rigidity after yield (kPa)
7.75×10^7	0.29	7.9	3.64×10^5	2.47×10^5

Linear plane elements with two degrees of freedom per node were used to model the pile cap and the superstructure mass.

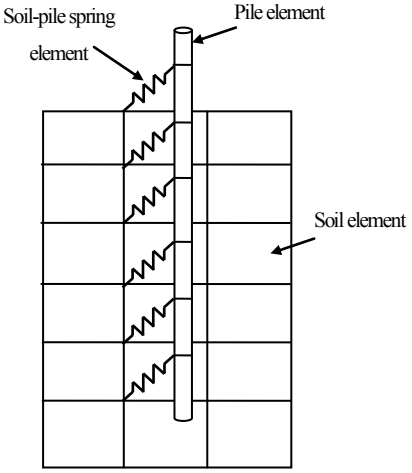

Fig. 4 Concept of a soil-pile spring element.

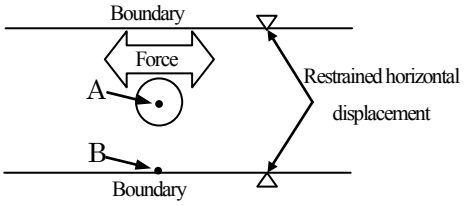

Fig. 5 Analysis domain for the soil-pile interaction

3.5 Pile-soil interaction spring

The interaction between a pile and the surrounding soil in 3-D was idealized using 2-D analysis. The nonlinear-spring element in Fig. 4 was used to represent the soil-pile interation. The underlying concept of this spring was to analyze soil deformation in the direction perpendicular to the direction of pile deflection. Parameters of the spring element were determined by parametric studies, using finite element method, on the soil-pile interaction in a 2-D horizontal plane as shown in Fig. 5. At the right and left side boundaries, displacements were fixed.

Parameters for the sand used for the analysis are shown in Table 7. The cylindrical pile section was idealized using linear solid elements.

Figure 6 shows the load-relative displacement relationship under cyclic loading where the relative displacement is defined as the difference in horizontal displacement between the center point of the pile (point A) and a point located at the boundary (point B). As a comparison, simple shear tests of a single element of soil were simulated using the same parameters of the dry sand as shown in Fig. 7 . The relationship between the load and relative displacement of a pile (Fig. 6) and the relationship between shear stress and shear strain of one element of dry sand (Fig. 7) were similar. Based on such similarities, the relationships between the relative displacement of a pile and the shear strain of a single soil element can be calibrated then the parameteres of soil-pile spring can be calculated from a simulation of simple shear tests of a single soil element as follows Ozutsumi et al. [15]:

$$\text{Shear strain} = u / (D \times \beta_p) \quad (13)$$

$$\text{Spring force} = (L \times D \times \alpha_p) \times \text{Shear stress} \quad (14)$$

where u, D, and L are the relative displacement, pile diameter, and pile length, respectively. Generally, the values for α_p and β_p depend on the type of soil, drained/undrained soil

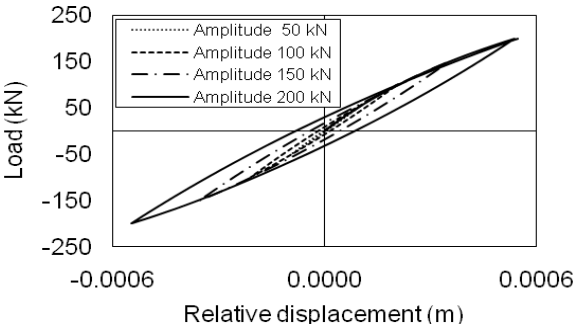

Fig. 6 Load-displacement relationship of pile-soil system in horizontal plane under cyclic loading

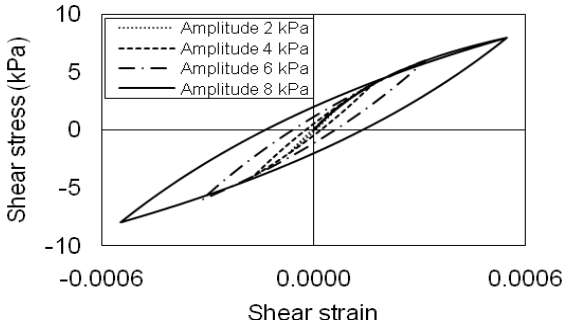

Fig.7 Shear stress-shear strain relationship of a single

condition, and the current load relative to the ultimate load of the pile. The values for α_p and β_p ranged 11.5-12.6 and 0.5-2.5, respectively. In the analysis, the values of these two parameters were determined automatically using the used program (**FLIP**) as a function of aformentioned factors. The phase difference between pile and soil movements was not taken into account.

4. Comparison of calculated and recorded responses

The challenge for the FE models was to reasonably approximate the recoreded responses for a total six cases (three input motion shaken the system with and without the superstructure mass) with the same model and the same soil proprties.

4.1. Time histories of the soil-pile-superstructure system

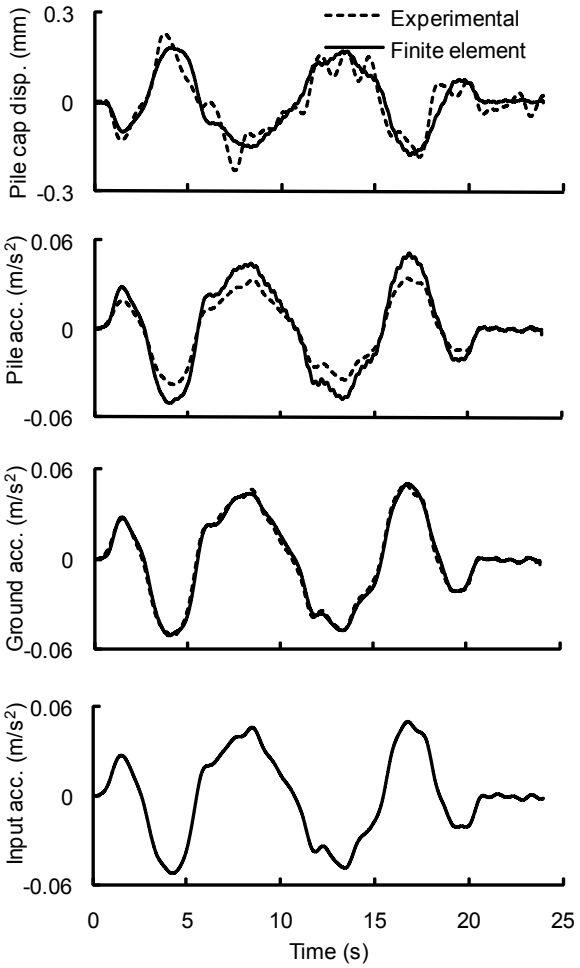

Fig. 8 Comparison of recorded and calculated ground and pile cap responses, without superstructure, 0.1 Hz

Recorded and calculated responses of soil and pile cap for input motions of 0.1, 0.5, and 1.0 Hz without the superstructure mass are compared in Fig. 8, 9, and 10, respectively. The computed time histories of ground acceleration, pile cap aceleration, and pile cap displacement are consistent with recorded ones in terms of their amplitudes and phases. Thus the FE analysis reproduced soil and pile cap responces reasonably

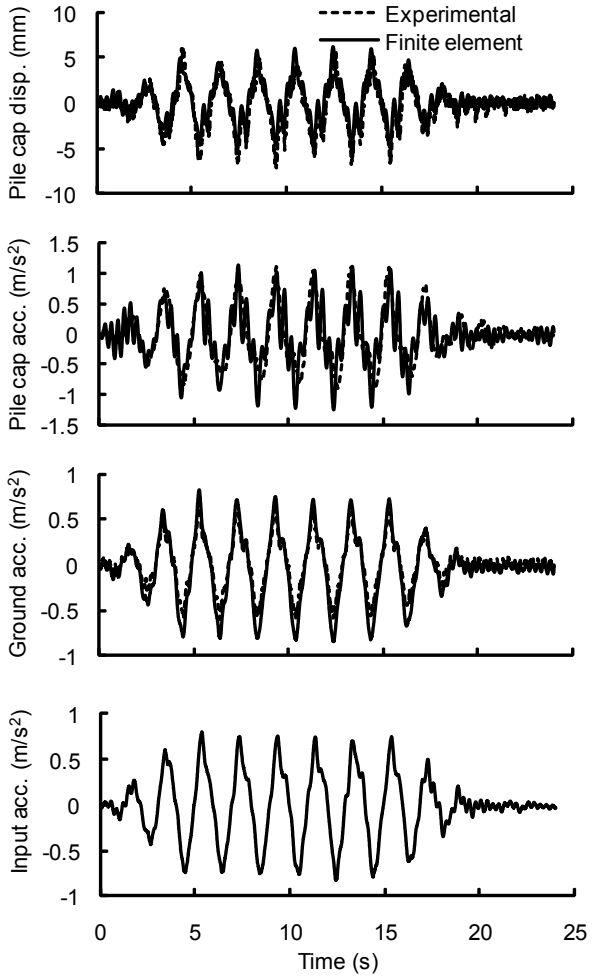

Fig. 9 Comparison of recorded and calculated ground and pile cap responses, without superstructure, 0.5 Hz

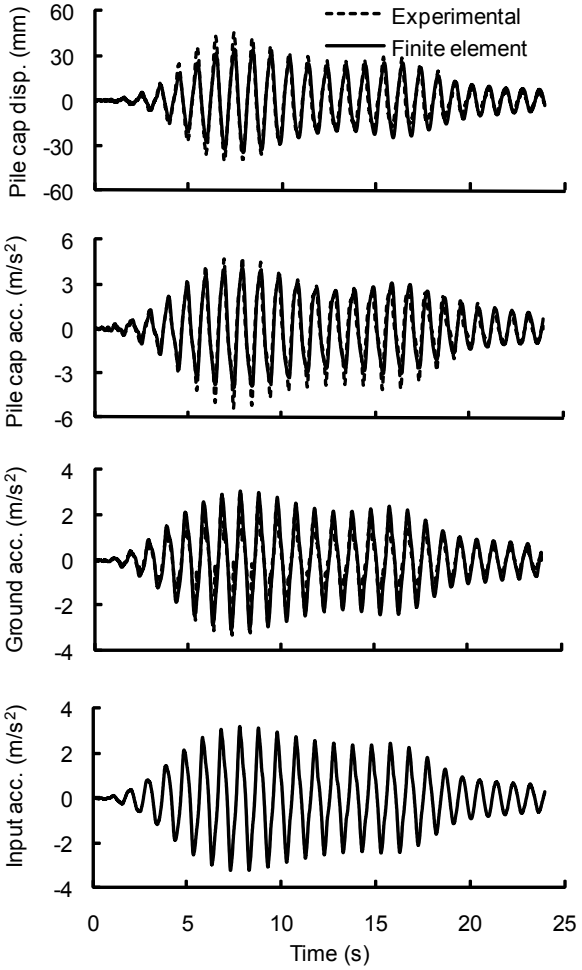

Fig. 10 Comparison of recorded and calculated ground and pile cap responses, without superstructure 1.0 Hz

well.

Recorded and calculated responses of soil, pile cap, and superstructure mass for input motions of 0.1, 0.5, and 1.0 Hz after adding the superstructure mass are compared in Fig. 11, 12, and 13, respectively. The general trend of ground acceleration, pile cap aceleration, and pile cap displacement records was satisfactorily predicted in terms of their amplitudes and phases for all input motions. The computed time histories of superstructure acceleration are consistent with the recorded in terms of phase for all input motions. However , the FE slightely underestimated the amplitudes of superstructure acceleration for input motion of 1.0 Hz. For input motions of 0.1 and 0.5 Hz, the computed superstructure accelerations agree well with the recorded one.

The soil and structural accelerations for 0.5 Hz input motion are presented in terms of Fourier spectra in Fig. 14, which show also that the FE analysis reproduced soil and structural accelerations that agree well with the measured data.

The effect of soil nonlinearity on the seismic response of the soil-pile-structure system are examined using the current numerical model.. Three sinusoidal waves as input base accelerations with different amplitudes as shown in Table 6 but with constant frequency of 0.5 Hz were applied to the system without superstructure (single degree of freedom structure). Fig 15 (a) shows the normalized Fourier amplitude (Fourier amplitude divided by max amplitude) of the input motions. The normalized Fourier amplitudes of the pile cap acceleration are plotted in Fig 15 (b). Fig 15 (c) shows the response of the pile cap focusing on the period from 0.2 to 0.6 s. It can be observed from Fig 15 (c) that the fundamental period of the system increases from 0.3 s at input motion of 0.005 g to 0.5 s at 0.317 g.. The increase of the fundamental period may be attributed to increased soil nonlinearity due to the inertial force.

4.2. Peak bending moment profile

Figures 16 and 17 plot the peak bending moment profiles, calculated as extreams bending-moments at different depthes along the pile for input motions of 0.1 and 1.0 Hz and for both cases with and without the

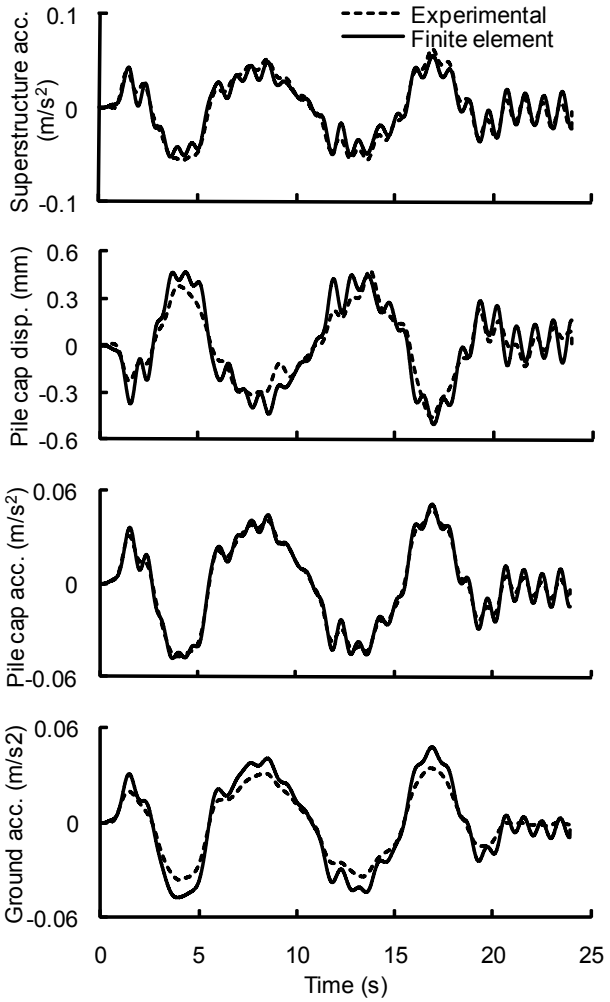

Fig. 11 Comparison of recorded and calculated ground and pile cap responses, with superstructure 0.1 Hz

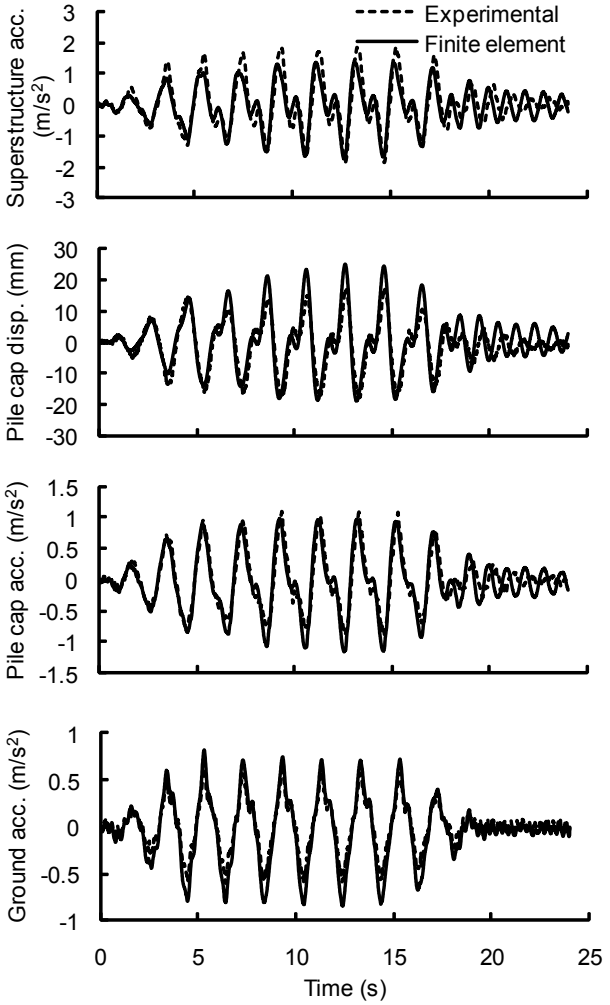

Fig. 12 Comparison of recorded and calculated ground and pile cap responses, with superstructure 0.5 Hz

superstructure mass. These figure compare the depths where the maximum moments were measured and computed. Although, the depth of computed maximum moment agreed well with the measured one at 0.1 Hz, there is a difference at 1.0 Hz and this difference was about 1.5 m. The computed depths where the bending moment returned to zero were consistent with the measured ones. The difference between the measured and computed depths was within 1.0 m.. For the system without the superstructure mass, the computed bending moment profile agreed well with the measured one at 0.1 and 1.0 Hz. The FE is also successful at predicting the increase of peak bending moment profile after adding the superstructure mass but the computed increase of bending moment differed from the recorded one and this may be due to the empirical procedure for the setting of soil-pile interaction springs. Some calibration in the numerical modeling may be required to have more consistent results on the bending moments

5. Conclusions

This paper presents a comparison between nonlinear seismic analyses using the 2-D finite element (FE) and the results of shaking table centrifuge model tests of pile-supported structures in a dense sand profile. The FE analyses were reasonably able to approximate the recorded responses during shaking in centrifuge tests for the range of conditions covered in the experiments. The challenge was to approximate the recorded responses for a total of six cases using a common set of modeling parameters. As illustrated by the representive time series , Fourier spectra , and bending moment profiles, the overall comparisions indicated that these FE models could now be used to parametrically evaluate the influnce of other key factors, such as varying structural periods, pile slenderness, soil-pile relative stiffness, and input motions.

References

1) Kagawa, T. and Kraft, L., Seismic P-Y responses of flexible piles, *Journal of Geotechnical Engineering, ASCE*, 106(8),

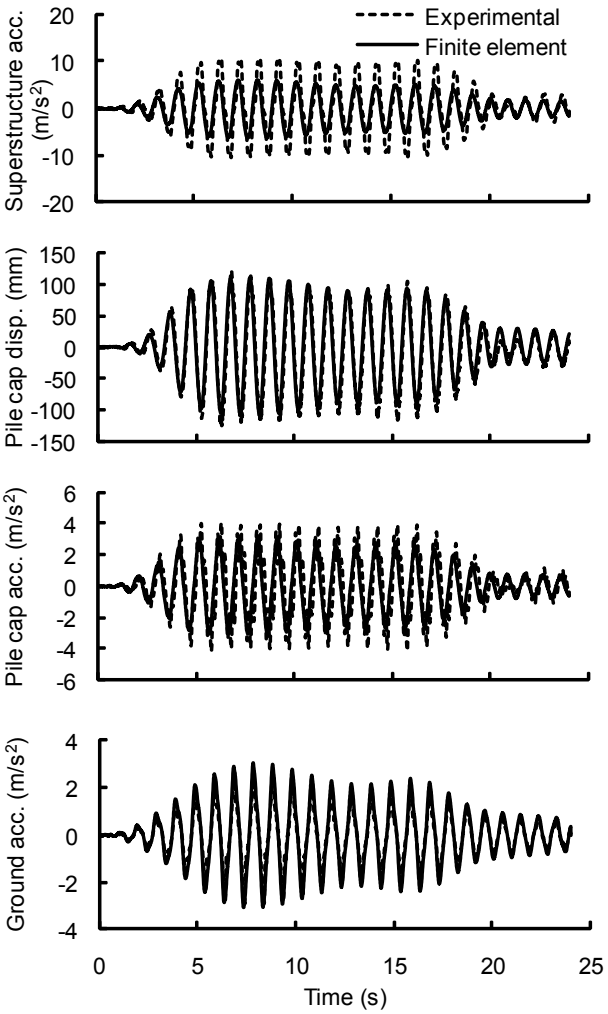

Fig. 13 Comparison of recorded and calculated ground and pile cap responses, with superstructure 1.0 Hz

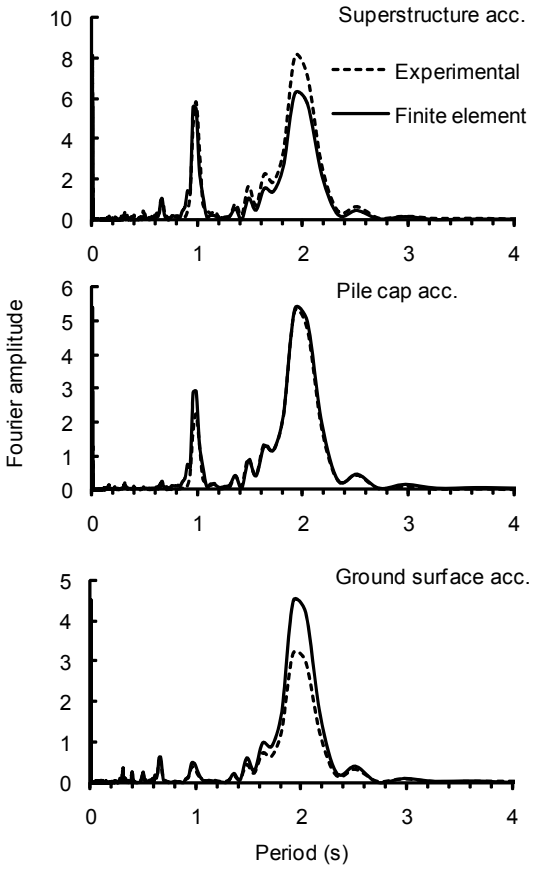

Fig. 14 Comparison of recorded and calculated Fourier spectra for ground, pile cap , and superstructure mass accelerations, 0.5 Hz

899-918, 1980.

2) Pender, M. and Pranjoto, S., Gapping effects during cyclic lateral loading of piles in clay, *Proc. 11th World Conf. Earthquake Eng., Acapulco,* Paper No. 1007. 1996.
3) Allotey, N. and El Naggar, M.H., Generalized dynamic Winkler model for nonlinear soil-structure interaction analysis, *Canadian Geotechnical Journal*, 45(4), 560-573, 2008.
4) Blaney, G., Kausel, E., Roesset, J., Dynamic stiffness of piles, *Proc. 2nd Intl. Conf. on Numerical Methods in Geomechanics, Blacksburg*, 1001-1012, 1976.
5) Cai, Y., Gould, P., Desai, C., Numerical implementation of a 3-D nonlinear seismic S-P-S-I methodology, in Seismic Analysis and Design for Soil-Pile-Structure Interactions, *Geotechnical Special Publication, 70, ASCE*, 96-110, 1995.
6) Rovithis, E.N., Pitilakis, K.D., Mylonakis, G.E., Seismic analysis of coupled soil-pile-structure systems leading to the definition of a pseudo-natural SSI frequency, *Soil Dynamics and Earthquake Engineering*, 29(6), 1005-1015, 2009.
7) Kattis, S.E., Polyzos, D., Beskos, D.E., Vibration isolation by a row of piles using a 3-D frequency domain BEM, *International Journal for Numerical Methods in Engineering*, 64, 713-728, 1999.
8) Padrón, J.A., Aznárez, J.J., Maeso, O., BEM–FEM coupling model for the dynamic analysis of piles and pile groups, *Engineering Analysis with Boundary Elements*, 31(6), 473-484, 2007.
9) Gazetas, G., Seismic response of end bearing single piles. *Soil Dynamics and Earthquake Engineering*, 3(2), 82–93, 1984.
10) Fan, K., Gazetas, G., Kaynia, A., Kausel, E., Ahmad, S., Kinematic seismic response of single piles and pile groups. *Journal of Geotechnical Engineering*, 117(12), 557–74, 1991.
11) Beltrami, C., Lai, C.G., Pecker, A., A kinematic interaction model for large diameter shaft foundation: An application to seismic demand assessment of a bridge subject to coupled swaying-rocking excitation. *Journal of Earthquake Engineering,* 9(2), 355–394, 2005.
12) Kaynia, A. M. and Mahzooni, S., Forces in pile foundations under seismic loading. *Journal of Engineering Mechanics*, 122(1), 46–53, 1996.
13) Mylonakis, G., Nikolaou, A., Gazetas, G., Soil-pile-bridge

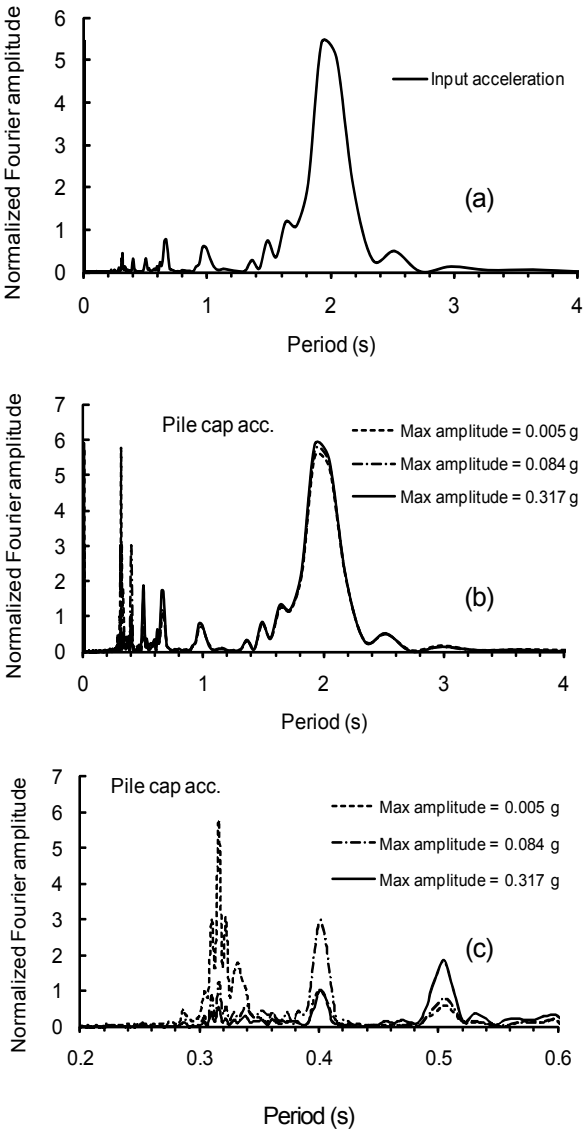

Fig. 15 Normalized Fourier spectra for input acceleration, pile cap accelerations, 0.5 Hz

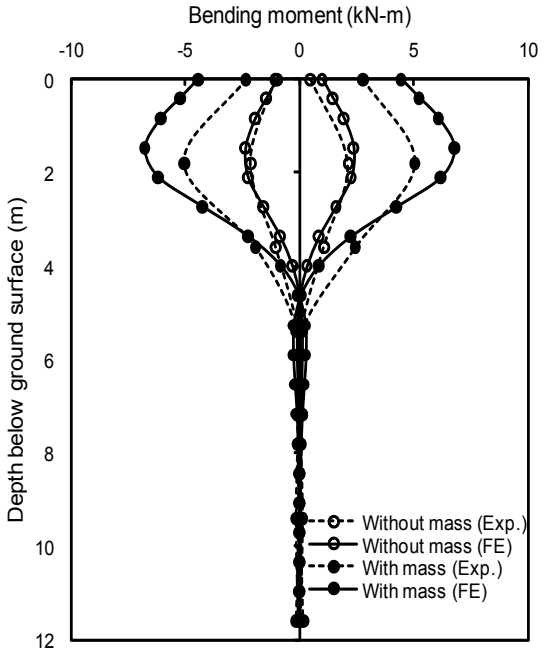

Fig. 16 Comparison of recorded and calculated peak bending moment profile, 0.1 Hz

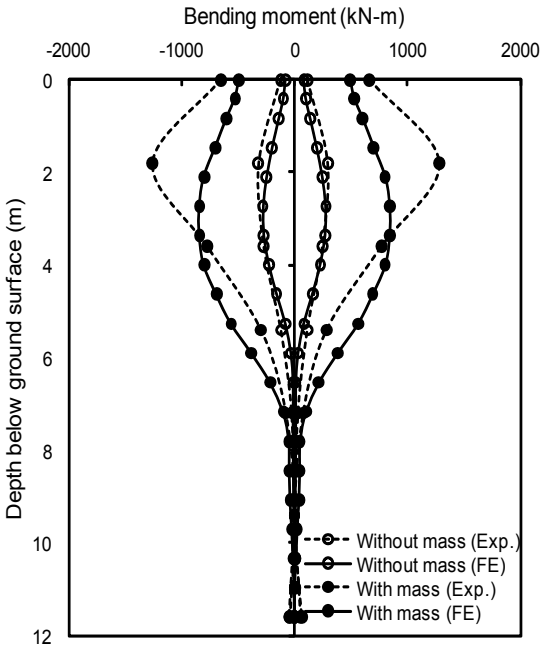

Fig. 17 Comparison of recorded and calculated peak bending moment profile, 1.0 Hz

seismic interaction: kinematic and inertial effects. Part I: Soft soil. *Earthquake Engineering and Structural Dynamics*, 26, 337–359, 1997.

14)Guin, J. and Banerjee, P. K., Coupled soil-pile-structure interaction analysis under seismic excitation. *Journal of Structural Engineering*, 124(4), 434–444, 1998.

15)Ozutsumi, O., Tamari, Y., Oka, Y., Ichii, K., Iai, S., Umeki, Y., Modeling of soil–pile interaction subjected to soil liquefaction in plane strain analysis, *Proc. of the 38th Japan National Conference on Geotechnical Engineering, Akita,*1899–1900, 2003.

16)Tamari, Y., Ozutsumi, O., Iai, S., Akutagawa, H., Effective stress dynamic analysis on the shaking table model test of piled foundation considering the dynamic interaction between pile and liquefied soil, Proc. Of the 42nd Japan National conference on Geotechnical Engineering, 1665-1666, 2007.

17)Tobita, T., Iai, S., Sugaya, M., Kaneko, H., Soil–pile interaction in horizontal plane: Seismic Performance and Simulation of Pile Foundations in Liquefied and Laterally Spreading Ground, *Geotechnical Special Publication*, *ASCE,* 145, 294–305, 2006.

18)Iai, S., Matsunaga, Y., Kameoka, T., Strain space plasticity model for cyclic mobility. *Soils and Foundations*, 32(2), 1–15, 1992.

(Received: March 9, 2010)